Communication

Additive Manufacturing of Co-Ni-Ga High-Temperature Shape Memory Alloy: Processability and Phase Transformation Behavior

C. LAUHOFF, A. FISCHER, C. SOBRERO, A. LIEHR, P. KROOß, F. BRENNE, J. RICHTER, M. KAHLERT, S. BÖHM, and T. NIENDORF

Co-Ni-Ga high-temperature shape memory alloy is additively processed by selective laser melting for the first time. Reversible martensitic transformation of the as-built material is proven by differential scanning calorimetry. Microstructural analysis reveals a columnar-grained microstructure resulting from epitaxial solidification. Columnar-grained microstructures are characterized by a very low degree of constraints being beneficial for superior functional performance in numerous shape memory alloys. However, process-induced crack formation remains a challenge towards robust realization of adequate conditions showing good mechanical properties.

https://doi.org/10.1007/s11661-019-05608-z

Binary Ni-Ti is currently the shape memory alloy (SMA) system of choice in many niche applications due to its good biocompatibility, high transformation strains and excellent cyclic stability. However, Ni-Ti SMAs suffer from limited transformation temperatures (TTs) and high production costs.[1–3] To extend the application temperature range, high-temperature (HT-) SMAs featuring increased martensite start temperatures (M_s) have been designed. These alloys enable new applications in the fields of aerospace, automotive, oil and gas as well as other industries.[4,5] Adding a third element to Ni-Ti is a common practice to increase the TTs.[4] Ni-Ti-Hf is currently the most promising HT-SMA being in focus of many studies.[6–8] However, high costs of the alloying elements as well as highly challenging processing and machining remain major roadblocks towards widespread use of Ni-Ti-Hf in industrial applications.[9,10]

Over the last decades, many alternative alloy systems have been introduced as HT-SMA candidates.[4,5] Among the alternative systems, the Heusler-type Co-Ni-Ga alloys have gained considerable attention[11]: Co-Ni-Ga, undergoing a martensitic transformation from cubic B2-ordered austenite to tetragonal $L1_0$ martensite,[12] consists of relatively inexpensive alloying elements and features excellent functional properties at elevated temperatures. In single-crystalline state, a fully reversible pseudoelastic response up to temperatures of about 500 °C and excellent functional stability at temperatures up to 100 °C have been shown.[13–15] This qualifies Co-Ni-Ga for high-temperature damping applications. Aging of stress-induced martensite, referred to as *SIM-aging*,[16] changes the chemical order and, thus, is suited to directly tailor the TTs. Hence, stable high-temperature actuation can be realized as well.[16,17] In addition, good formability can be obtained by controlled segregation of the ductile secondary γ-phase (A1).[18–21]

The fundamental properties of this alloy system are characterized in depth. However, excellent functional properties have been reported mainly for single-crystalline material so far. Owing to a pronounced anisotropic transformation behavior and a limited number of martensite variants, deformation constraints at grain boundaries (GB) cannot be sufficiently accommodated in polycrystalline material with random texture. Eventually, premature failure, *i.e.*, intergranular fracture upon thermo-mechanical processing and/or loading is commonly observed.[4,19,22] Even grain boundary engineering *via* segregation of the highly ductile γ-phase along the GBs is not capable to fully prevent cracking of unfavorable GBs in polycrystalline Co-Ni-Ga structures upon martensitic phase transformation.[22,23] Thus, the key towards superior shape memory performance in such relatively brittle and anisotropic SMAs is the presence of microstructures being characterized by a very low degree of grain constraints.[24–26] Triple junctions have been proven to be the most detrimental microstructural feature leading to rapid structural and functional degradation.[26] In line with those findings, a columnar-grained microstructure, featuring a strong ⟨001⟩ texture and geometrically absolutely straight GBs of low-angle character, has been proposed to overcome these issues in case of a Cu-based SMA.[27,28] A different approach aims at realization of oligocrystals, also referred to as bamboo-like structures, in which the

C. LAUHOFF, A. FISCHER, A. LIEHR, P. KROOß, J. RICHTER, M. KAHLERT, and T. NIENDORF are with the Institute of Materials Engineering, University of Kassel, 34125 Kassel, Germany. Contact e-mail: lauhoff@uni-kassel.de C. SOBRERO is with the Institute of Physics Rosario (CONICET), Rosario's National University, 2000 Rosario, Argentina. F. BRENNE is with the Institute of Materials Engineering, University of Kassel and also with the Department of Mechanical Science and Engineering, University of Illinois at Urbana-Champaign, Urbana, IL 61801. S. BÖHM is with the Institute of Production Technologies and Logistics, University of Kassel, 34125 Kassel, Germany.

Manuscript submitted August 14, 2019.
Article published online January 6, 2020

GBs exceed the entire cross section of the sample and are mainly oriented perpendicular to the loading axis.[24,25] Despite the obvious differences between both microstructures, *i.e.*, columnar-grained and bamboo-like structures, the low degree of constraints is found to be vital for obtaining superior functional properties in polycrystalline SMAs, being competitive to those of their single-crystalline counterparts.[19,24,27,29]

Recently, the group of Kainuma introduced a promising cyclic heat treatment to control the grain size in SMAs by abnormal grain growth (AGG).[30] So far, AGG induced by a cyclic heat treatment has been observed for Cu-Al-Mn[30,31] and Fe-Mn-Al-Ni-X[32,33] SMAs, leading to oligocrystalline grain structures or even single crystals in the range of several centimeters. In a very recent study, a novel thermo-mechanical processing route for promoting AGG in polycrystalline Co-Ni-Ga HT-SMAs was introduced.[20,21] Hot extrusion followed by a post-processing heat treatment led to the formation of bamboo structures evoking enhanced functional performance. Nonetheless, as processing remains highly challenging, alternative procedures providing for microstructures with minimized grain constraints have to be established.

In this regard, additive manufacturing (AM) processes are highly attractive, as these techniques allow for direct microstructure design.[34,35] One of the most common AM techniques for processing of metallic materials is the powder bed-based selective laser melting (SLM) process. During SLM, a laser system is used to melt a pre-alloyed powder layer by layer according to data provided by a computer-aided design file. A direct microstructural design is achieved by controlling the thermal gradient and the solidification velocity, which in turn can be adjusted by the processing parameters, such as laser power, scanning velocity, hatch distance and scanning pattern.[36] As has been shown for various materials, strongly textured columnar-grained microstructures can be obtained by SLM.[36–39] However, no work has been published on AM of Co-Ni-Ga in the literature so far, although direct microstructure design is highly promising for obtaining excellent functional material properties in this system. To close this gap, the current study focuses on the SLM processability of a Co-Ni-Ga HT-SMA. Microstructure and martensitic phase transformation behavior of the SLM processed material have been thoroughly investigated. The general feasibility of direct microstructure design, *i.e.*, realization of a columnar-grained microstructure, is reported. Critical steps towards robust processing of the alloy are highlighted.

In the current study, a SLM machine SLM280^{HL} employing a 400 W laser was used for fabrication of samples from a Co-Ni-Ga SMA with a nominal composition of 49Co-21Ni-30Ga (in at. pct). This composition is designed for good shape memory properties with a high degree of strain recoverability.[15] The chemical composition of the initial as-cast material was 48.9 Co, 21.0 Ni and 30.1 Ga (in at. pct) as determined by X-ray fluorescence analysis (XRF). Co-Ni-Ga SMA powder with a particle size ranging from 20 to 52 μm was obtained by gas atomization of the as-cast material, which was carried out by TLS Technik (Bitterfeld, Germany). Chemical composition of the powder material was determined using energy-dispersive X-ray spectroscopy (EDS). $10 \times 10 \times 15$ mm^3 cubes were manufactured with a layer thickness of 50 μm and a hatch distance of 0.12 mm under argon atmosphere at 110 °C. The laser operated at a nominal power of 175 W and a scan velocity of 650 mm s^{-1}, resulting in an energy density of 45 J mm^{-3}. A bidirectional scanning strategy with 90 deg rotation between successive layers was employed for fabrication of all cubes. In the light of robust processing as well as the desired microstructure characterized by a low degree of constraints, the employed scanning strategy is suitable to reduce process-induced residual stresses[40,41] and, concurrently, known to be beneficial for evolution of pronounced texture during processing.[36]

The as-built cubes were cut by electrical discharge machining (EDM) along and perpendicular to the building direction (BD). Samples were ground down to 5 μm grit size to remove the EDM-affected surface layer. Following grinding, samples were mechanically polished for 1 h using a colloidal SiO_2 suspension with 0.02 μm particle size. For microstructure characterization, optical microscopy (OM) as well as scanning electron microscopy (SEM) including EDS were employed. For OM, samples were etched using a solution of 33 ml ethanol, 8.5 ml H_20, 50 ml HCl and 8.5 g Cu_2S. For phase analysis, synchrotron radiation and a PerkinElmer (XRD1621) area detector were employed at the P02.1 high-resolution powder diffraction beamline (DESY synchrotron facility, Hamburg, Germany). Using synchrotron diffraction sample volumes of several mm^3 can be probed and a detailed high-resolution microstructure analysis is enabled. A wavelength of 0.02072926 nm was used. For further details on the synchrotron beamline P02.1 the reader is referred to Reference 42. Defect analysis within the sample volume was carried out using a Zeiss X-radia 520 Versa computed tomography system with sub-micron resolution (μ-CT). For the investigation a sample volume of $2 \times 2 \times 4$ mm^3 was scanned. The μ-CT operated at 80 kV. For analysis a sub-volume of $1750 \times 1750 \times 3150$ μm^3 was extracted from the scanned sample volume to avoid surface effects. The voxel size was set to 3.9 μm. Differential scanning calorimetry (DSC) was used to investigate the martensitic phase transformation behavior. DSC was conducted using a Mettler-Toledo DSC 1 calorimeter at heating and cooling rates of 10 K min^{-1}.

Figure 1 shows synchrotron diffraction patterns obtained at room temperature from the initial Co-Ni-Ga powder and the SLM as-built condition. The powder particles are fully austenitic with a B2-type ordered bcc lattice, as determined from the peaks at diffraction angles between 4.5 and 13 deg (Figure 1(a)). The lattice parameter of the B2 austenite is $a = 2.865$ Å. The powder particles following gas atomization are characterized by high sphericity and a very small fraction of adhering satellites (inset in Figure 1(a)). Following AM the material features a dual-phase microstructure, as can be deduced from the additional peaks in the diffraction

pattern (Figure 1(b)). In addition to the austenitic phase with $a = 2.858$ Å, tetragonal martensite is present. The crystal structure of the martensitic phase is $L1_0$ with lattice parameters of $a = 2.711$ Å and $c = 3.170$ Å. All lattice parameters are in accordance with data in literature.[12,43] The slight deviation between the austenitic lattice parameters can be attributed to process-induced residual stresses and minor changes in chemical composition, as will be detailed hereafter. The dual-phase microstructure appears as a lath like austenite-martensite relief in the individual grains (see inset in Figure 1(b)) similar to that of as-cast Co-Ni-Ga alloys in References 44 and 45.

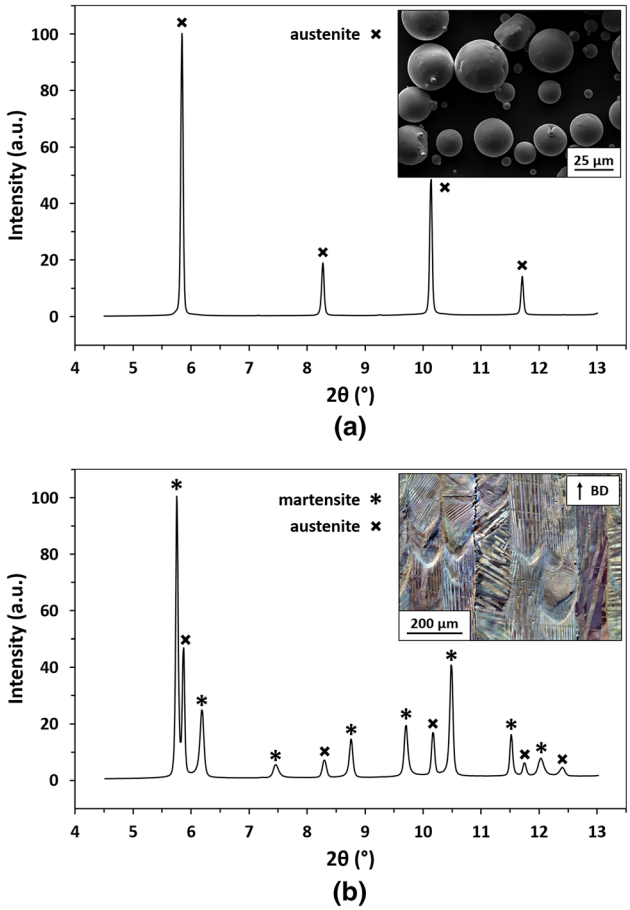

Fig. 1—Synchrotron diffraction patterns of Co-Ni-Ga powder (*a*) and the SLM processed material (*b*) in the as-built condition. The SEM and Argus image in the insets show the powder particles (a) and the as-built microstructure (b), respectively.

The optical micrographs in Figures 2(a) and (b) depict the microstructure of the as-built material parallel and perpendicular to BD, respectively. Columnar grains with long axes in the millimeter range grow parallel to BD (Figure 2(a)). Owing to the partial re-melting of the underlying solid material, epitaxial solidification is promoted in the SLM process.[36,38] Thus, the resulting grain long axes are clearly larger than the initial layer thickness. Although epitaxial grain growth across individual layers was reported for various SLM-fabricated materials,[36–39,46,47] the strong columnarity of the as-built Co-Ni-Ga is remarkable. This is further highlighted by the grain structure resolved perpendicular to BD (Figure 2(b)). Due to the bidirectional scanning strategy in combination with the 90 deg rotation applied, a checkerboard-like grain arrangement is formed, as also observed in *e.g.*,References 38 and 47 for Ta and Ni-Ti, respectively. Liu *et al.*[27,28] found an almost perfect pseudoelastic behavior in columnar-grained microstructures with strong crystallographic texture and absolutely straight low-energy GBs in Cu-based SMAs. In addition, even if no strong texture is present, enhanced functional properties and excellent resistance against GB cracking were shown by the current authors in a very recent study for both bamboo-like and columnar-grained Co-Ni-Ga bi-crystals.[22] Consequently, additive manufacturing *via* SLM is thought to be highly promising to obtain Co-Ni-Ga HT-SMAs with appropriate microstructures featuring excellent resistance to functional and structural degradation.

Results from μ-CT shown in Figure 3 reveal substantial crack formation in the columnar-grained SLM Co-Ni-Ga. A relative density of 85.6 pct has been determined from these results. It has to be noted that in a preceding laser parameter study material of significantly higher density, *i.e.*, free of cracks, was

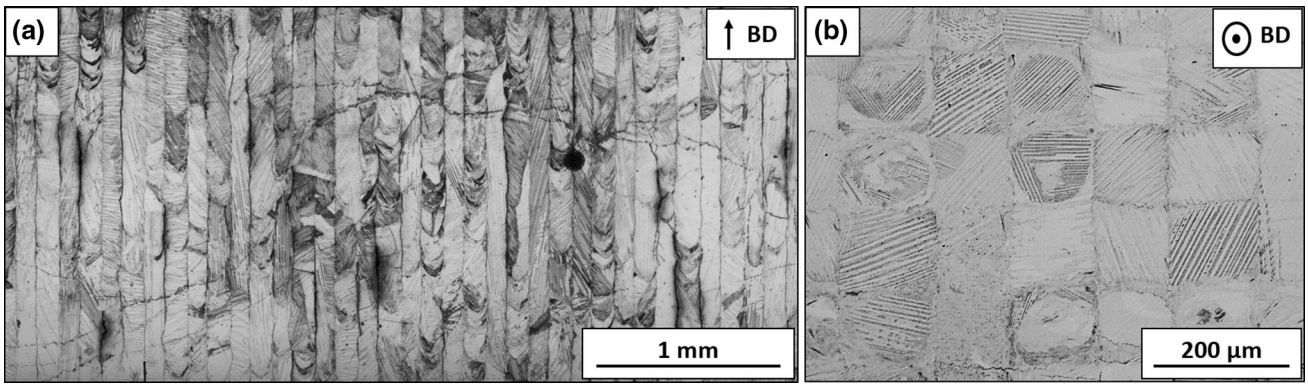

Fig. 2—Optical micrographs revealing the microstructure of Co-Ni-Ga processed by SLM in the as-built condition. The images represent the side view (*a*) and the top view (*b*) of the manufactured cubes, as indicated by the arrows labeled BD.

obtained. However, those conditions were characterized by an unfavorable globular and fine-grained microstructure (not shown). For the sake of brevity, only the set of processing parameters leading to favorable microstructural features is presented in the present paper. The cracks depicted in Figure 3 are mainly oriented parallel to the laser scanning vectors during processing. The reason for this phenomenon is seen to be rooted in residual stresses, which typically are formed due to repeated heating, solidification and rapid cooling during layer-wise processing,[48] leading to phenomena such as hot and cold cracking. In addition, owing to the high cooling rates being characteristic for the process, precipitation of the ductile secondary γ-phase along the GBs is not observed, as can be deduced from synchrotron data (Figure 1(b)) and the optical micrographs (Figure 2). This phase has been proven to be of highest importance for hindering intergranular crack nucleation and propagation.[22,23] The unfavorable combination of the thermally induced stresses and the high brittleness of the as-built material probably leads to cracking alongside the GBs during the SLM process. A parameter optimization including base plate heating up to 600 °C is currently under consideration to obtain crack-free material, which simultaneously shows the desired microstructural features. Increasing the base plate temperature is very promising to reduce the process-induced residual stresses in hard to process alloys as has been shown for, *e.g.*, tool steels.[50] Furthermore and in light of the cost efficiency of the AM process, the adjustment of the process-related parameters to avoid process-induced defects should be in focus of future work instead of using well-established post-process treatments, such as hot isostatic pressing (HIP). However, further process parameter optimization is clearly beyond the scope of the present work.

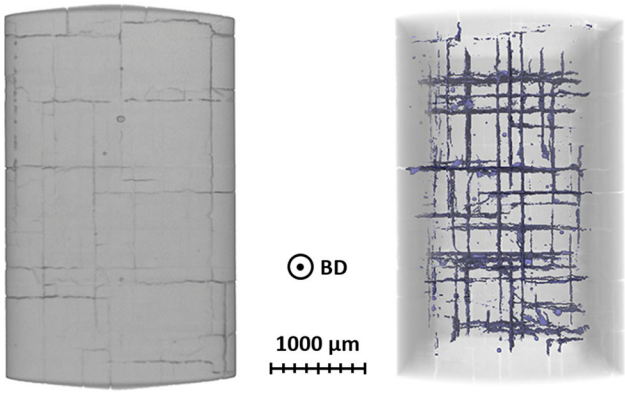

Fig. 3—Computed tomography analysis of as-built Co-Ni-Ga showing substantial crack formation after SLM fabrication: 2D image of a single plane (left), 3D visualization (right).

The thermal phase transformation characteristics of as-processed Co-Ni-Ga, revealed by DSC analysis, are shown in Figure 4. The endothermic and exothermic reactions associated with the forward and reverse martensitic transformation can be clearly identified in the DSC curve upon heating and cooling, respectively. The TTs of the as-built condition, determined using the tangent method, were found to be M_s = 77 °C, M_f = 34 °C, A_s = 50 °C and A_f = 95 °C. It is important to note that the synchrotron phase analysis (Figure 1(b)) and the optical micrographs (Figure 2) of the as-built material revealed an austenitic-

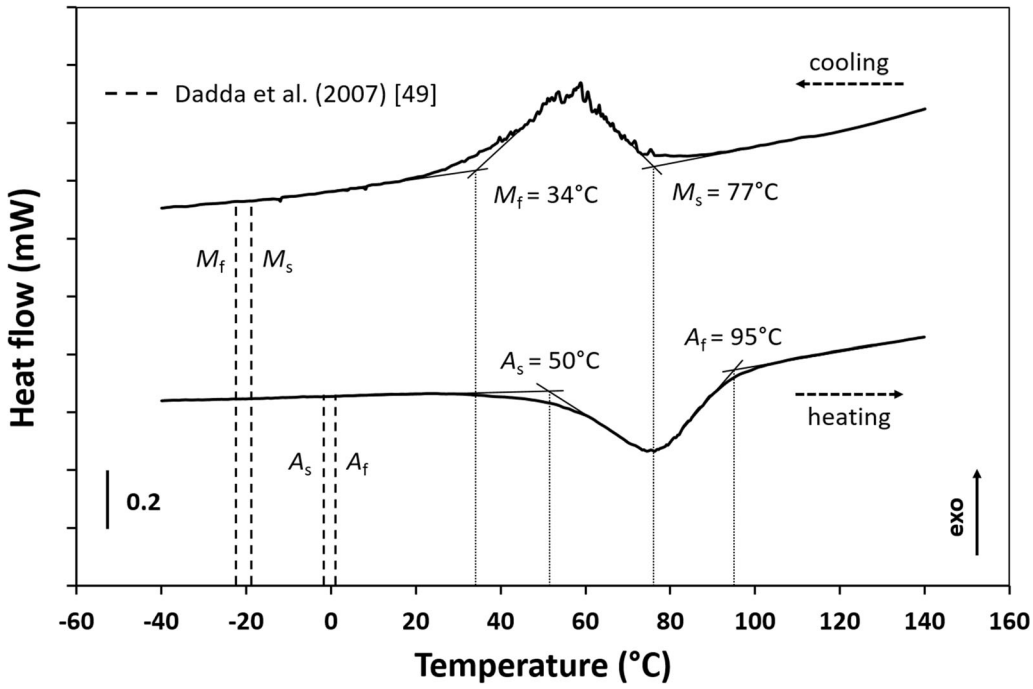

Fig. 4—DSC curve for SLM processed Co-Ni-Ga in the as-built condition. The characteristic transformation temperatures upon heating (A_s and A_f) and cooling (M_s and M_f) are marked. In addition, transformation temperatures of single-crystalline $Co_{49}Ni_{21}Ga_{30}$ recompiled from Ref. [49] are highlighted by dashed lines.

martensitic dual-phase microstructure at room temperature, *i.e.*, M_f below RT. The slight difference in TTs as compared to the DSC results (M_f = 34 °C) could be due to minor inhomogeneity in the microstructure, slight differences in local chemical composition and/or the internal stress state.[49] At this point, it has to be emphasized that the material utilized in this study was not homogenized after SLM processing. In addition, samples for DSC had to be cut and polished, at least leading to a change of the residual stress state. Quantitative evaluation of the impact of each single parameter, however, is clearly beyond the scope of the present study and, thus, has to be subject of future work.

Still, the DSC results indicate that the absolute TTs as well as the temperature ranges for forward and reverse transformation, *i.e.*, $\Delta_1 = A_f - A_s$ and $\Delta_2 = M_s - M_f$, are significantly increased compared to single-crystalline $Co_{49}Ni_{21}Ga_{30}$.[49] The increase of Δ_1 and Δ_2 is mainly attributed to the polycrystalline state and grain constraints, respectively. The increase in TTs is further thought to be rooted in a general change in chemical composition. Increased Ni and decreased Ga contents have been reported to lead to higher M_s in the Co-Ni-Ga system.[44,51] In the present study, the Ga content in the as-built material was found to be about 1.0 at. pct below that of both the initial as-cast as well as the powder material (as determined by EDS). Thus, the increase in TTs is mostly attributed to the evaporation of the volatile element Ga during SLM processing. As shown by Elahinia *et al.*[8] for a Ni-Ti-Hf HT-SMA, evaporation of nickel and oxygen pick-up are very influential to the transformation behavior of SMAs. Further factors contributing the shift of TTs and the increase of the transformation temperature ranges Δ_1 and Δ_2 (as compared to the single-crystalline material) might be process-induced defects, such as inclusions and cracks, as shown for Ni-Ti.[52] Obviously, the latter ones are very prominent in the microstructure under investigation. In contrast to the Ni-Ti-based alloys being very sensitive to the alloy composition in terms of the TTs, however, adequate post heat treatments seem to offer more efficient pathways for property optimization in Co-Ni-Ga.[16,17,44]

In conclusion, the current study demonstrates for the first time the processability of Co-Ni-Ga HT-SMAs *via* SLM. Reversibility of the martensitic transformation and characteristic TTs have been revealed by DSC. By choosing a suitable set of processing parameters, a favorable microstructure is obtained directly after processing. Epitaxial growth leads to an anisotropic, columnar microstructure being very attractive for enhanced functional properties in polycrystalline SMA systems. Thus, it is expected that AM of hard to form Co-Ni-Ga will open up new possibilities to overcome major roadblocks toward application. Avoidance of severe processing-induced defects needs to be addressed in future studies to evaluate the thermo-mechanical functional properties in more detail.

Financial support by Deutsche Forschungsgemeinschaft (Project No. 250216343; NI1327/7-3) within the Emmy Noether-Program is gratefully acknowledged. DESY (Hamburg, Germany), a member of the Helmholtz Association HGF, is thanked for the provision of experimental facilities at the photon beamline P02.1 and the support laboratory. The authors gratefully acknowledge the assistance of Christian Staab with the DSC experiments.

REFERENCES

1. K. Otsuka and C.M. Wayman: *Shape Memory Materials*, Cambridge University Press, Cambridge, 1999.
2. K. Otsuka and X. Ren: *Prog. Mater Sci.*, 2005, vol. 50, pp. 511–678.
3. D.C. Lagoudas: *Shape Memory Alloys*, Springer, Boston, MA, 2008.
4. J. Ma, I. Karaman, and R.D. Noebe: *Int. Mater. Rev.*, 2013, vol. 55, pp. 257–315.
5. G.S. Firstov, J. van Humbeeck, and Y.N. Koval: *Mater. Sci. Eng. A*, 2004, vol. 378, pp. 2–10.
6. H. Sehitoglu, L. Patriarca, and Y. Wu: *Curr. Opin. Solid State Mater. Sci.*, 2017, vol. 21, pp. 113–20.
7. H. Sehitoglu, Y. Wu, and L. Patriarca: *Scripta Mater.*, 2017, vol. 129, pp. 11–15.
8. M. Elahinia, N. Shayesteh Moghaddam, A. Amerinatanzi, S. Saedi, G.P. Toker, H. Karaca, G.S. Bigelow, and O. Benafan: *Scripta Mater.*, 2018, vol. 145, pp. 90–94.
9. D. Biermann, F. Kahleyss, E. Krebs, and T. Upmeier: *J. of Materi Eng and Perform*, 2011, vol. 20, pp. 745–51.
10. M.H. Wu: *Mater. Sci. Forum*, 2002, vols. 394–395, pp. 285–92.
11. K. Oikawa, T. Ota, F. Gejima, T. Ohmori, R. Kainuma, and K. Ishida: *Mater. Trans.*, 2001, vol. 42, pp. 2472–75.
12. A. Reul, C. Lauhoff, P. Krooß, M.J. Gutmann, P.M. Kadletz, Y.I. Chumlyakov, T. Niendorf, and W.W. Schmahl: *Shap. Mem. Superelast.*, 2018, vol. 4, pp. 61–69.
13. P. Krooß, T. Niendorf, P.M. Kadletz, C. Somsen, M.J. Gutmann, Y.I. Chumlyakov, W.W. Schmahl, G. Eggeler, and H.J. Maier: *Shap. Mem. Superelasticity*, 2015, vol. 1, pp. 6–17.
14. J.A. Monroe, I. Karaman, H.E. Karaca, Y.I. Chumlyakov, and H.J. Maier: *Scripta Mater.*, 2010, vol. 62, pp. 368–71.
15. J. Dadda, H.J. Maier, I. Karaman, H.E. Karaca, and Y.I. Chumlyakov: *Scr. Mater.*, 2006, vol. 55, pp. 663–66.
16. T. Niendorf, P. Krooß, C. Somsen, G. Eggeler, Y.I. Chumlyakov, and H.J. Maier: *Acta Mater.*, 2015, vol. 89, pp. 298–304.
17. C. Lauhoff, P. Krooß, D. Langenkämper, C. Somsen, G. Eggeler, I. Kireeva, Y.I. Chumlyakov, and T. Niendorf: *Funct. Mater. Lett.*, 2018, vol. 11, art. no. 1850024.
18. E. Dogan, I. Karaman, Y.I. Chumlyakov, and Z.P. Luo: *Acta Mater.*, 2011, vol. 59, pp. 1168–83.
19. M. Vollmer, P. Krooß, C. Segel, A. Weidner, A. Paulsen, J. Frenzel, M. Schaper, G. Eggeler, H.J. Maier, and T. Niendorf: *J. Alloys Compd.*, 2015, vol. 633, pp. 288–95.
20. E. Karsten, G. Gerstein, O. Golovko, A. Dalinger, C. Lauhoff, P. Krooss, T. Niendorf, A. Samsonenko, and H.J. Maier: *Shap. Mem. Superelasticity*, 2019, vol. 5, pp. 84–94.
21. T. Niendorf, C. Lauhoff, E. Karsten, G. Gerstein, A. Liehr, P. Krooß, and H.J. Maier: *Scripta Mater.*, 2019, vol. 162, pp. 127–31.
22. C. Lauhoff, M. Vollmer, P. Krooß, I. Kireeva, Y.I. Chumlyakov, and T. Niendorf: *Shap. Mem. Superelast.*, 2019, vol. 5, pp. 73–83.
23. R.D. Dar, H. Yan, and Y. Chen: *Scr. Mater.*, 2016, vol. 115, pp. 113–17.
24. Y. Sutou, T. Omori, R. Kainuma, and K. Ishida: *Acta Mater.*, 2013, vol. 61, pp. 3842–50.
25. S.M. Ueland, Y. Chen, and C.A. Schuh: *Adv. Funct. Mater.*, 2012, vol. 22, pp. 2094–99.
26. S.M. Ueland and C.A. Schuh: *J. Appl. Phys.*, 2013, vol. 114, art. no. 053503.
27. J.-L. Liu, H.-Y. Huang, and J.-X. Xie: *Mater. Des*, 2014, vol. 64, pp. 427–33.

28. J.-L. Liu, H.-Y. Huang, J.-X. Xie, S. Xu, and F. Li: *Scripta Mater*., 2017, vol. 136, pp. 106–10.
29. T. Omori, M. Okano, and R. Kainuma: *APL Mater*., 2013, vol. 1, art. no. 032103.
30. T. Omori, T. Kusama, S. Kawata, I. Ohnuma, Y. Sutou, Y. Araki, K. Ishida, and R. Kainuma: *Science*, 2013, vol. 341, pp. 1500–02.
31. T. Kusama, T. Omori, T. Saito, S. Kise, T. Tanaka, Y. Araki, and R. Kainuma: *Nat. Commun*., 2017, vol. 8, p. 354.
32. T. Omori, H. Iwaizako, and R. Kainuma: *Mater. Des*., 2016, vol. 101, pp. 263–69.
33. M. Vollmer, T. Arold, M.J. Kriegel, V. Klemm, S. Degener, J. Freudenberger, and T. Niendorf: *Nat. Commun*., 2019, vol. 10, art. no. 2337.
34. T. Niendorf, F. Brenne, M. Schaper, A. Riemer, S. Leuders, W. Reimche, D. Schwarze, and H.J. Maier: *Rapid Prototyp. J*., 2016, vol. 22, pp. 630–35.
35. T. Niendorf, S. Leuders, A. Riemer, F. Brenne, T. Tröster, H.A. Richard, and D. Schwarze: *Adv. Eng. Mater*., 2014, vol. 16, pp. 857–61.
36. L. Thijs, K. Kempen, J.-P. Kruth, and J. van Humbeeck: *Acta Mater*., 2013, vol. 61, pp. 1809–19.
37. T. Niendorf, S. Leuders, A. Riemer, H.A. Richard, T. Tröster, and D. Schwarze: *Metall. Mater. Trans. B*, 2013, vol. 44B, pp. 794–96.
38. L. Thijs, M.L. Montero Sistiaga, R. Wauthle, Q. Xie, J.-P. Kruth, and J. van Humbeeck: *Acta Mater*., 2013, vol. 61, pp. 4657–68.
39. F. Brenne, A. Taube, M. Pröbstle, S. Neumeier, D. Schwarze, M. Schaper, and T. Niendorf: *Prog. Addit. Manuf*., 2016, vol. 1, pp. 141–51.
40. T. Simson, A. Emmel, A. Dwars, and J. Böhm: *Addit. Manuf*., 2017, vol. 17, pp. 183–89.
41. M.F. Zaeh and G. Branner: *Prod. Eng. Res. Devel*., 2010, vol. 4, pp. 35–45.
42. A.-C. Dippel, H.-P. Liermann, J.T. Delitz, P. Walter, H. Schulte-Schrepping, O.H. Seeck, and H. Franz: *J. Synchrotron Radiat*., 2015, vol. 22, pp. 675–87.
43. P.M. Kadletz, P. Krooß, Y.I. Chumlyakov, M.J. Gutmann, W.W. Schmahl, H.J. Maier, and T. Niendorf: *Mater. Lett*., 2015, vol. 159, pp. 16–19.
44. J. Liu, M. Xia, Y. Huang, H. Zheng, and J. Li: *J. Alloys Compd*., 2006, vol. 417, pp. 96–99.
45. M. Wuttig, J. Li, and C. Craciunescu: *Scripta Mater*., 2001, vol. 44, pp. 2393–97.
46. L. Thijs, F. Verhaeghe, T. Craeghs, J. van Humbeeck, and J.-P. Kruth: *Acta Mater*., 2010, vol. 58, pp. 3303–12.
47. T. Bormann, B. Müller, M. Schinhammer, A. Kessler, P. Thalmann, and M. de Wild: *Mater. Charact*., 2014, vol. 94, pp. 189–202.
48. P. Mercelis and J.-P. Kruth: *Rapid Prototyp. J*., 2006, vol. 12, pp. 254–65.
49. J. Dadda, D. Canadinc, H.J. Maier, I. Karaman, H.E. Karaca, and Y.I. Chumlyakov: *Philos. Mag*., 2007, vol. 87, pp. 2313–22.
50. B. Breidenstein, F. Brenne, L. Wu, T. Niendorf, and B. Denkena: *HTM J. Heat Treatm. Mat*., 2018, vol. 73, pp. 173–86.
51. K. Oikawa, T. Ota, Y. Imano, T. Omori, R. Kainuma, and K. Ishida: *JPED*, 2006, vol. 27, pp. 75–82.
52. M. Speirs, B. van Hooreweder, J. van Humbeeck, and J.-P. Kruth: *J. Mech. Behav. Biomed. Mater*., 2017, vol. 70, pp. 53–59.